PHYSICAL REVIEW B VOLUME 47, NUMBER 4 15 JANUARY 1993-II

Band structure and symmetry analysis of coherently grown $Si_{1-x}Ge_x$ alloys on oriented substrates

Q. M. Ma and K. L. Wang
Device Research Laboratory, Department of Electrical Engineering, University of California at Los Angeles, Los Angeles, California 90024

J. N. Schulman
Hughes Research Laboratory, Malibu, California 90265

(Received 18 November 1991; revised manuscript received 16 September 1992)

A semiempirical tight-binding method was used to calculate the band structures of $Si_{1-x}Ge_x$ alloys coherently grown on (001)-, (111)-, and (110)-oriented $Si_{1-y}Ge_y$ substrates. The distorted lattice and Brillouin zone, as well as the band-edge splittings and shifts which vary with the Ge content of both the $Si_{1-x}Ge_x$ strained layer and the substrate, are given. The band structures and symmetry properties of the coherently strained $Si_{1-x}Ge_x$ alloys along high-symmetry lines of the distorted Brillouin zone are analyzed. The calculation results show that for the [001] and [111] growth cases, the conduction-band minima appear in the growth direction when the epilayer is under tensile strain. When the $Si_{1-x}Ge_x$ alloys are grown on a (111)- or (110)-oriented substrate, the four-degree degenerate state X_5 in the [001] direction of an unstrained diamond structure splits into two bands with even and odd parities, respectively. This splitting results in a nonlinear effect, which increases rapidly with increasing strain and results in the downward bending of $E_c^{\Delta}(6)$ and $E_c^{\Delta}(2)$ for Si-rich alloys grown on (111) and (110) Ge substrates, respectively. This effect deviates from the band-edge variation trend given by linear deformation-potential theory, which does not explicitly include the nonlinear effect. Corresponding to the reduced symmetry of the distorted diamond structures, irreducible representations of the space groups are obtained and used to denote the calculated energy bands. Relations among the irreducible representations of the energy bands, such as compatibility, the relation between energy bands of unstrained and strained diamond structures, and additional degeneracies due to time-reversal symmetry, are obtained and shown. Finally, selection rules for direct optical transitions are obtained within the framework of the electric-dipole approximation, and the effects of the polarization of incident light are discussed.

I. INTRODUCTION

Recently, there has been increasing interest in electronic properties of Si/Ge strained-layer quantum wells and superlattices[1-4] and their application to electronic and optical devices. The band structure, which is fundamental to the electronic properties, is distorted under strain. People[5,6] and others have used linear deformation-potential theory to predict the band-edge shifts and splittings of coherently strained $Si_{1-x}Ge_x$ alloys. But the exact nature and the symmetry properties of the distorted band structures in the Brillouin zone remain unclear. Moreover, since the deformation-potential values were obtained in external stress experiments, where the strain tensors were relatively small, nonlinear effects due to high strain as in typical cases of coherent growth need further study. A semiempirical tight-binding method can be used to calculate the band structures in the distorted Brillouin zone, which automatically incorporates the full space group of the strained $Si_{1-x}Ge_x$ alloy (as a virtual crystal). Using the tight-binding technique, band mixing, crossing or anticrossing, degeneracy and spin-orbit splittings can all be included.

In this paper, the semiempirical tight-binding method including the strain is used as described in Sec. II. The consideration of symmetry properties and the irreducible representations are given in Sec. III. Section IV presents the calculation results for the band-edge variations with the Ge content of the strained layer and the substrate, and the band structures and symmetry properties of coherently grown $Si_{1-x}Ge_x$ alloys on (001)-, (111)-, and (110)-oriented $Si_{1-y}Ge_y$ substrates. Finally, the selection rules for direct optical transitions are discussed in Sec. V.

II. TIGHT-BINDING METHOD AND STRAIN

A. Tight-binding calculation of $Si_{1-x}Ge_x$ alloy

A semiempirical tight-binding method was used to calculate the band structure of the $Si_{1-x}Ge_x$ bulk alloy. Interactions among the nearest and second-nearest atoms were considered and sp^3 orbitals of each atom were taken as the basis functions. Spin-orbit splitting was also taken into account according to the method given in Refs. 7 and 8. Slater-Koster integral parameters[9] were adopted and the parameters used for bulk Si and Ge are given in Table I. For the $Si_{1-x}Ge_x$ alloy, the virtual-crystal approximation was used, in which the integral parameters of the alloy were the linear interpolations of those of bulk Si and Ge:

TABLE I. Two-center integral parameters for bulk Si and Ge determined by fitting to experimental data and pseudopotential calculations. The subscripts 1 and 2 designate nearest and second-nearest interactions. All parameters are in units of eV.

Integral parameters	Si	Ge
$E_{ss}(000)$	0.0	0.0
$E_{xx}(000)$	4.380	5.524
$(ss\sigma)_1$	−2.094	−1.679
$(sp\sigma)_1$	1.687	1.819
$(pp\sigma)_1$	2.250	2.010
$(pp\pi)_1$	−0.483	−0.405
$(ss\sigma)_2$	0.001	−0.030
$(sp\sigma)_2$	0.0948	−0.086
$(pp\sigma)_2$	0.483	0.369
$(pp\pi)_2$	−0.060	0.011

$$E_{pq}(\mathrm{Si}_{1-x}\mathrm{Ge}_x)=xE_{pq}(\mathrm{Ge})+(1-x)E_{pq}(\mathrm{Si})\ , \qquad (1)$$

where E_{pq} is the two-center integral parameter between orbitals p and q. Shen *et al.*[10] used a nonlinear interpolation for the integral parameters of alloys, but in our calculation we prefer the linear interpolation.

In order to see the strain effect on the band structures of $\mathrm{Si}_{1-x}\mathrm{Ge}_x$ alloys, the band structures of unstrained Si and Ge along different directions of the Brillouin zones were first calculated and shown in Figs. 1 and 2, in which the band structures along the eight ⟨111⟩ directions are the same, and so are the bands along the six ⟨100⟩ directions. It will be shown later that these equivalent bands may be split or shifted by the coherent strain. The band structures in Figs. 1 and 2 agree with those of other calculations.[11] Although for the higher conduction bands the data are not very accurate in the present calculation, the lower conduction-band edges are very close to the experimental data[12] and are given as follows:

	$\Gamma_{\min}$	$\Delta_{\min}$	L
Si:	3.38	1.12	1.80
Ge:	0.77	0.87	0.66

The band structures of $\mathrm{Si}_{1-x}\mathrm{Ge}_x$ alloys, calculated using Eq. (1) and the tight-binding parameters of Si and Ge, show a gradual transformation from Si to Ge when the alloy changes from pure Si to pure Ge (i.e., x increases from 0.0 to 1.0). Figure 3 shows the variation of direct and indirect optical transition energies of the $\mathrm{Si}_{1-x}\mathrm{Ge}_x$ alloy as a function of the Ge content x, where $E_0=E_c(\Gamma_7^-)-E_c(\Gamma_8^+),E_0'=E_c(\Gamma_6^-)-E_c(\Gamma_8^+)$ are two direct transition energies at the Γ point; $E_{g,d}(X)$ and $E_{g,d}(L)$ are the minimum direct transition energies at the X and L points, respectively. The minimum indirect transition $E_{g,i}(\Delta,L)$ is compared with the experimental value $E_{g,i}(\exp)$. One can see from Fig. 3 that when the Ge content of the alloy increases from 0.0 to 1.0, E_0 (or the Γ_7^- band of Fig. 1) decreases, crosses the E_0' (or the Γ_6^- band) at about $x=0.3$, and becomes the lowest conduction band at the Γ point for $x>0.3$. At the same time, the two lowest conduction bands, L_6^+ at the L point and Δ_6 in the Δ line of Fig. 1, also decrease but with different rates. These two indirect minimum-energy values are equal at about $x=0.77$ and then L_6^+ becomes the lowest conduction band for $x>0.77$ shown in Fig. 3. The indirect-gap energy $E_{gi}(\Delta,L)$ is the minimum of the two described above. The calculated results are in agreement with other calculations[13] and experimental data,[12] except the cross-point value $x_c=0.77$, which is smaller than the experimental result of 0.85. The low value of x_c in the present calculation is due to the fact that the energy value (1.8 eV) of the L-point minimum of bulk Si is lower than the experimental data (2.0 eV). This may also have some effect on the accuracy of the L-point minimum of a coherently grown $\mathrm{Si}_{1-x}\mathrm{Ge}_x$ alloy.

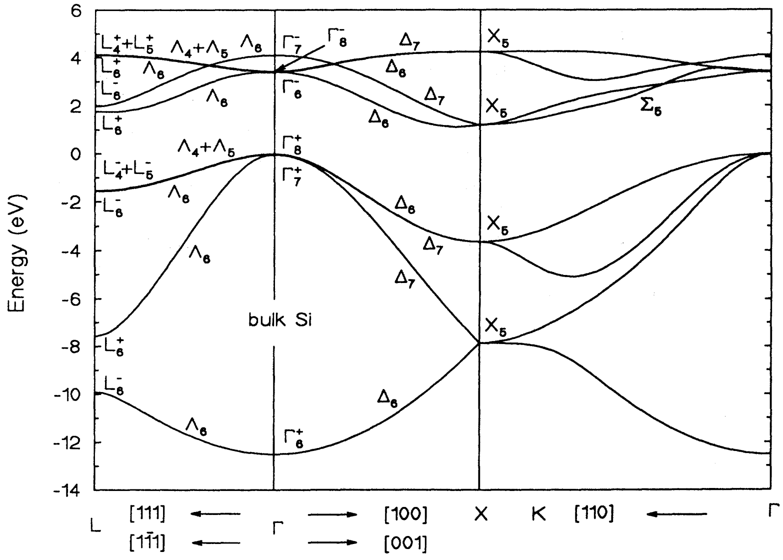

FIG. 1. Band structure of bulk Si.

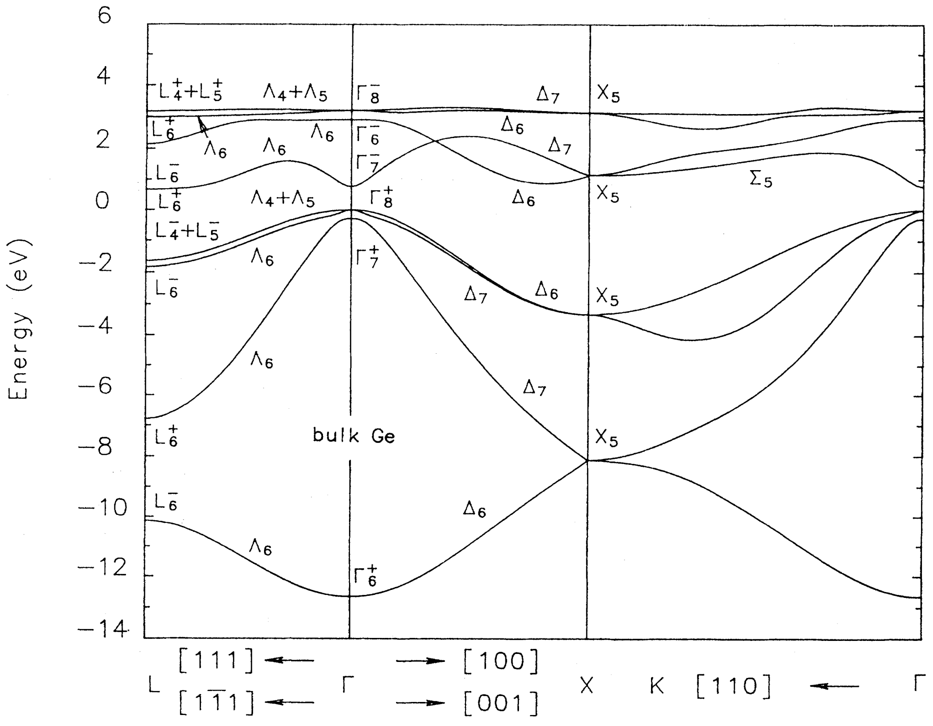

FIG. 2. Band structure of bulk Ge.

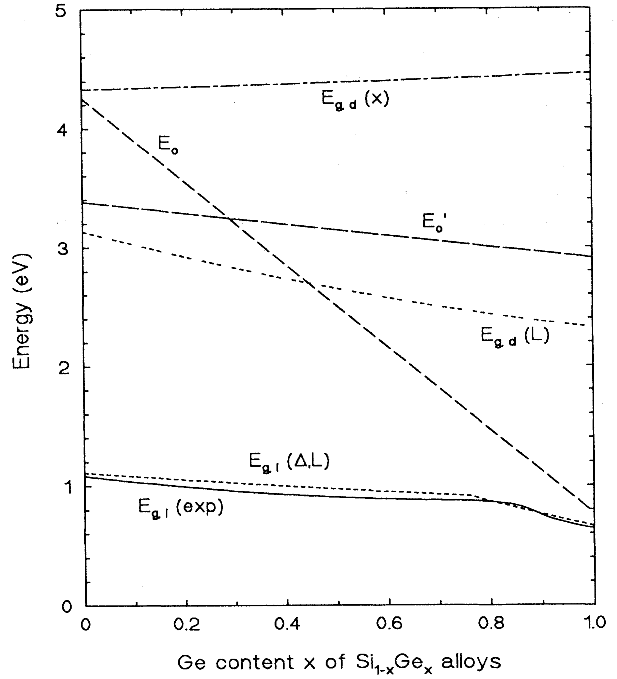

FIG. 3. Direct and indirect band gaps of a bulk $Si_{1-x}Ge_x$ alloy. E_0 is the energy difference between Γ_7^- and Γ_8^+, E_0' is the energy difference between Γ_6^- and Γ_8^+, $E_{g,d}(X)$ and $E_{g,d}(L)$ are the direct band gaps at points X and L, respectively, $E_{g,i}(\Delta,L)$ is the indirect band gap from the Δ line into the L point, and $E_{g,i}(\exp)$ is the experimental data of the indirect band gap given in Ref. 12.

B. Strain considerations

In the coherent growth of $Si_{1-x}Ge_x$ alloys on a $Si_{1-y}Ge_y$ substrate, internal stress and strain will build up due to the lattice mismatch. The strain tensor for a coherently grown epilayer is similar to that when the alloy is under an external biaxial stress. The strain tensor components ϵ_{xx}, ϵ_{yy}, and ϵ_{zz} denote the relative displacements in the three coordinate directions x, y, and z, while ϵ_{xy}, ϵ_{xz} and ϵ_{yz} denote one-half of the changes in the angle between two originally perpendicular lines. In our calculation, the strain is assumed to be elastic and homogeneous.

Based on the elastic properties of bulk Si and Ge, the strain and stress tensors can be easily obtained in a growth coordinate system $OX'Y'Z'$, where OZ' is taken as the growth direction. By coordinate transformation, the strain tensors can be represented in the conventional crystal coordinate system of the diamond structure, $OXYZ$, where OX, OY, OZ are taken along the $\langle 100 \rangle$ symmetry directions of the crystal. The strain tensors for the [001], [111], and [110] growth cases are given in the $OXYZ$ coordinate system as follows:

[001] growth:

$$\epsilon_{001} = \begin{bmatrix} \epsilon_{xx} & 0 & 0 \\ 0 & \epsilon_{xx} & 0 \\ 0 & 0 & \epsilon_{zz} \end{bmatrix} , \tag{2}$$

where

$$\epsilon_{xx}=\epsilon'_x \ , \quad \epsilon_{zz}=-2\frac{C_{12}}{C_{11}}\epsilon'_x \ .$$

[111] growth:

$$\epsilon_{111}=\begin{bmatrix} \epsilon_{xx} & \epsilon_{xy} & \epsilon_{xy} \\ \epsilon_{xy} & \epsilon_{xx} & \epsilon_{xy} \\ \epsilon_{xy} & \epsilon_{xy} & \epsilon_{xx} \end{bmatrix} , \tag{3}$$

where

$$\epsilon_{xx}=\frac{4C_{44}}{4C_{44}+C_{11}+2C_{12}}\epsilon'_x \ ,$$

$$\epsilon_{xy}=\frac{-(C_{11}+2C_{12})}{4C_{44}+C_{11}+2C_{12}}\epsilon'_x \ .$$

[110] growth:

$$\epsilon_{110}=\begin{bmatrix} \epsilon_{xx} & \epsilon_{xy} & 0 \\ \epsilon_{xy} & \epsilon_{xx} & 0 \\ 0 & 0 & \epsilon_{zz} \end{bmatrix} , \tag{4}$$

where

$$\epsilon_{xx}=\frac{2C_{44}-C_{12}}{2C_{44}+C_{11}+C_{12}}\epsilon'_x \ ,$$

$$\epsilon_{zz}=\epsilon'_x \ ,$$

$$\epsilon_{xy}=\frac{-(C_{11}+2C_{12})}{2C_{44}+C_{11}+C_{12}}\epsilon'_x \ ,$$

where $\epsilon'_x=(a_s-a_0)/a_0$ is the strain tensor component in the growth plane, a_s is the lattice constant of the substrate, and a_0 is the lattice constant of the unstrained layer. The values of the elastic stiffness constants C_{11}, C_{12}, and C_{44} (10^{11} dyn cm^{-1}) are taken as follows:[14,15]

	C_{11}	C_{12}	C_{44}
Si:	16.577	6.393	7.962
Ge:	12.40	4.13	6.83

For the [001] and [111] growth cases, the strain and stress components in the growth plane have relations $\epsilon'_x=\epsilon'_y$, $T'_x=T'_y$, respectively, where ϵ'_x, ϵ'_y, T'_x, and T'_y are the strain and stress components in the OX' and OY' directions in the growth plane. For the [110] growth case, it can be shown that the relation, $\epsilon'_x=\epsilon'_y$ holds while $T'_x\neq T'_y$. Due to the latter, the strain tensor cannot be decomposed into the sum of the strain tensors of a pure hydrostatic pressure and a uniaxial stress for the [110] growth case.

C. Distorted lattice and Brillouin zone

In the coherent growth of a $Si_{1-x}Ge_x$ alloy, the diamond structure is distorted differently according to the growth direction as are the Bravais lattice and the Brillouin zone. Within the range of elastic strain, the atom's position in the distorted Bravais lattice is given by

$$\mathbf{R}_i^A=(1+\epsilon)\mathbf{R}_{i,0}^A \ , \tag{5}$$

where $\mathbf{R}_{i,0}^A$ and $\mathbf{R}_i^A$ are the atom's position in sublattice A of the unstrained and strained diamond structures, respectively, 1 is the unit tensor and ϵ is the strain tensor. When the $Si_{1-x}Ge_x$ alloy is coherently grown on a (001)-oriented substrate, the atoms of both sublattices A and B of the diamond structure are distorted according to Eq. (5). But, if the growth direction is along the [111] or [110] direction, there is an additional internal displacement between the atoms of the two sublattices. This internal displacement is usually described by the "internal-strain parameter" ζ,[16] varying from 0 to 1.0. The values $\zeta_{Si}=0.53$ and $\zeta_{Ge}=0.44$ (Ref. 17) for Si and Ge, respectively, were used in our calculation for the [111] and [110] growth cases.

If the location of an atom in sublattice A of the distorted diamond structure is described by Eq. (5), the coordinate of an atom in sublattice B is given by the following:[18,19]

[001] growth:

$$\mathbf{R}_i^B=(1+\epsilon)\mathbf{R}_{i,0}^B \ , \tag{6}$$

[111] growth:

$$\mathbf{R}_i^B=(1+\epsilon)\mathbf{R}_{i,0}^B-\frac{a_0}{2}\epsilon_{xy}\zeta\begin{bmatrix}1\\1\\1\end{bmatrix} , \tag{7}$$

[110] growth:

$$\mathbf{R}_i^B=(1+\epsilon)\mathbf{R}_{i,0}^B-\frac{a_0}{2}\epsilon_{xy}\zeta\begin{bmatrix}0\\0\\1\end{bmatrix} , \tag{8}$$

where $\mathbf{R}_{i,0}^B$ and $\mathbf{R}_i^B$ are similar denotations for sublattice B, a_0 is the lattice constant of the unstrained diamond structure, and ϵ_{xy} is the strain tensor component given in Eqs. (3) and (4).

The undistorted and distorted diamond structures calculated from Eqs. (5)–(8) are shown in Fig. 4 for Ge grown on (001)-, (111)-, and (110)-oriented Si substrates. From the relations between the basis of the crystals and their reciprocal lattices, the distorted Brillouin zones were calculated and shown in Fig. 5. In order to clearly illustrate the distortion, the strain used in Figs. 4 and 5 is fictitiously made four times larger than the true strain of a Ge layer grown on a Si substrate. The symbols denoting high-symmetry points and lines of the distorted Brillouin zones in Figs. 5(b)–5(d) are different from those of the unstrained diamond structure in Fig. 5(a), because the new Bravais lattice is no longer face-centered-cubic, and the symbols correspond to the Brillouin zones of the new Bravais lattices.[20]

By analyzing the change of the symmetry of the Brillouin zones, the following results can be obtained. For the [001] growth case, the original six equivalent {100} faces in Fig. 5(a) are distorted and fall into two groups in Fig. 5(b): four faces (100), $(\bar{1}00)$, (010), and $(0\bar{1}0)$ in one group, and (001) and $(00\bar{1})$ in the other. On the other hand, the equivalence of the eight {111} faces is unchanged. For the [111] growth case, Fig. 5(c) shows that the six {100} faces remain equivalent while the eight {111} faces are divided into two groups: (111) and $(\bar{1}\,\bar{1}\,\bar{1})$ in one group and six others in one group. For the [110] growth case, the six {100} faces of Fig. 5(d) are divided into two kinds: (001) and $(00\bar{1})$ are equivalent, (100), $(\bar{1}00)$, (010), and $(0\bar{1}0)$ are equivalent. The eight {111} faces are also divided into two kinds: (111), $(\bar{1}\,\bar{1}\,\bar{1})$, $(11\bar{1})$, and $(\bar{1}\,\bar{1}1)$ in one group; $(1\bar{1}1)$, $(\bar{1}1\bar{1})$, $(\bar{1}11)$, and $(1\bar{1}\,\bar{1})$ in the other. These new nonequivalent faces of the distorted Brillouin zones indicate the reduction of the symmetry of the band structures. Therefore, the conduction-band minima along these **k** directions are split as follows (referred to as interband splitting):

[001] growth:

$$E_c^{\Delta}(6)\Longrightarrow\begin{cases}E_c^{\Delta}(2):[001],[00\bar{1}] & \text{(in growth direction)}\\ E_c^{\Delta}(4):[100],[\bar{1}00],[010],[0\bar{1}0] & \text{(in growth plane)}\ ,\end{cases}$$

[111] growth:

$$E_c^{L}(4)\Longrightarrow\begin{cases}E_c^{L}(1):[111] & \text{(in growth direction)}\\ E_c^{L}(3):[\bar{1}11],[1\bar{1}1],[11\bar{1}] & \text{(in growth plane)}\ ,\end{cases}$$

[110] growth:

$$E_c^{\Delta}(6)\Longrightarrow\begin{cases}E_c^{\Delta}(2):[001],[00\bar{1}] & \text{(in growth plane)}\\ E_c^{\Delta}(4):[100],[\bar{1}00],[010],[0\bar{1}0]\ ,\end{cases}$$

$$E_c^{L}(4)\Longrightarrow\begin{cases}E_c^{L}(2):[111],[11\bar{1}]\\ E_c^{L}(2):[\bar{1}11],[1\bar{1}1]\ .\end{cases}$$

The above interband splitting pictures obtained from the argument of the symmetry change of the first Brillouin zone are reflected in our band-structure calculation results discussed in Sec. IV.

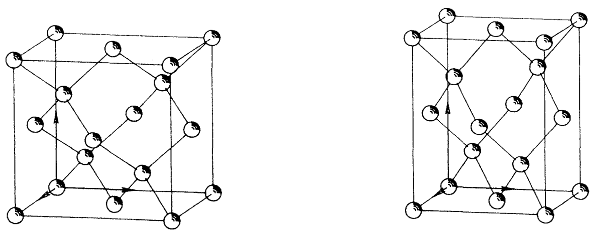

(a) bulk Si or Ge (b) Ge on (001) Si

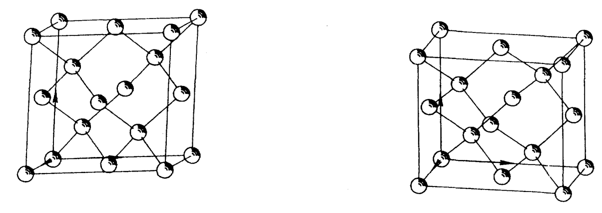

(c) Ge on (111) Si (d) Ge on (110) Si

FIG. 4. Distorted diamond structures coherently grown on oriented substrates: (a) unstrained diamond structure, (b) Ge grown on a (001) Si substrate, (c) Ge grown on a (111) Si substrate, and (d) Ge grown on a (110) Si substrate.

D. Strain and tight-binding parameters

In order to calculate the band structures of coherently grown $Si_{1-x}Ge_x$ alloys by the tight-binding method, there are two kinds of parameters that need to be adjusted with strain: the geometrical factors discussed above and the two-center integral parameters. In the well-known Harrison's law,[21] a two-center integral parameter has a d^{-2} dependence on the distance between two atoms. Although this law provides a reasonable general trend, it has been shown[22] that a more refined one can provide better results. The following modified Harrison's law is used to describe the integral dependence on the distance:[23]

$$E_{pq}=E_{pq}^{0}\left[\frac{d_0}{d}\right]^{n_{pq}}\ , \tag{9}$$

where E_{pq} is the two-center integral parameter with strain and E_{pq}^{0} is that without strain; similarly, d and d_0 are the distances between the two atoms with and without strain, respectively. In Eq. (9), n_{pq} is a parameter describing how the two-center integral changes with distance and it is orbital dependent. In the current calculation, eight such parameters are taken into consideration and the values are given below:

$$n_{ss}^{(1)}=4.77\ ,\quad n_{ss}^{(2)}=2.0,$$

$$n_{sp}^{(1)}=1.91\ ,\quad n_{sp}^{(2)}=1.0\ ,$$

$$n_{pp\sigma}^{(1)}=1.0\ ,\quad n_{pp\sigma}^{(2)}=3.1\ ,$$

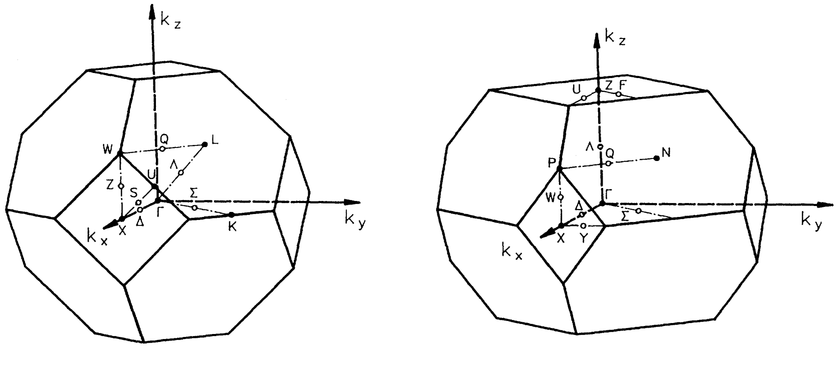

(a) bulk Si (b) Ge on (001) Si

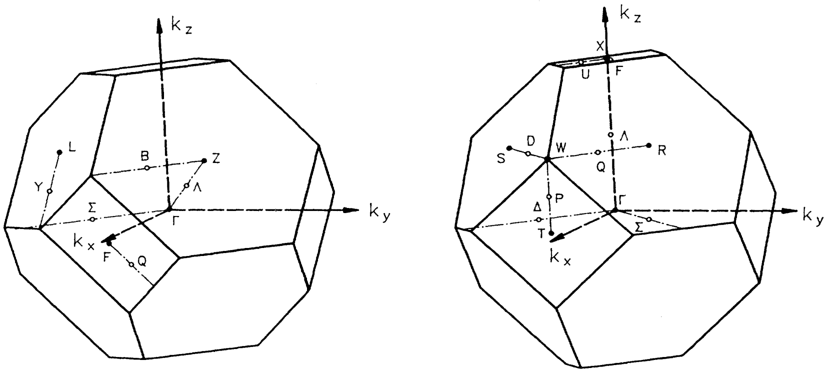

(c) Ge on (111) Si (d) Ge on (110) Si

FIG. 5. Distorted Brillouin zone of the coherently strained diamond structures grown on oriented substrates: (a) bulk Si and Ge, (b) Ge grown on a (001) Si substrate, (c) Ge grown on a (111) Si substrate, and (d) Ge grown on a (110) Si substrate.

$$n_{pp\pi}^{(1)}=2.2\ ,\quad n_{pp\pi}^{(2)}=1.5\ .$$

In the above forms, the superscripts (1) and (2) denote the nearest and second-nearest interactions. The above listed values of n_{pq} were obtained by continuing adjustment until the calculated band-edge variation with hydrostatic pressure fits best to the experimental data.[24] The major constraints in adjusting parameters are the band-edge variations at Γ, Δ, X, and L points. Since this method cannot determine the values of n_{pq} uniquely, the accuracy of the above n_{pq} parameters were analyzed by comparing the band-edge variations of bulk Si and Ge under hydrostatic pressure and [001], [111], and [110] uniaxial stress. The band-edge variations were calculated using the current method and compared with those obtained by the linear deformation-potential theory,[25,26] where the deformation potentials were taken as shown in Table II.

The comparison shows that when the hydrostatic pressure is under 4×10^4 kg/cm^2, the band-gap difference between the two methods is smaller than 0.02 eV. Similarly, when the uniaxial stress along the [001], [111], and [110] directions are under 9×10^3 kg/cm^2, the differences between the linear deformation-potential calculations[26,25] and our calculation for the direct and indirect band gaps at all the Γ, X, and L points are smaller than 0.03 eV. The agreement indicates that the n_{pq} parameters adjusted in our calculation are reasonable for the band-edge variations of Si and Ge under coherent strain. Thus Eqs. (1) and (9) were used throughout our calculation for the integral parameters of $Si_{1-x}Ge_x$ alloys, coherently grown on (001)-, (111)-, and (110)-oriented substrates.

III. STRAIN EFFECT ON SYMMETRY

One of the main characteristics of the coherently grown $Si_{1-x}Ge_x$ layers is that strain lifts the symmetry of the diamond structure, as shown in Fig. 4. Therefore, the space groups and the irreducible representations which denote the new energy bands will be different from those of an unstrained diamond structure.

According to group theory,[29,30] the symmetry operation of a space group G can be denoted as $\{\alpha|\mathbf{t}\}$, where α is a point-symmetry operation—rotation, reflection, inversion, etc.; $\mathbf{t}$ is a translational vector, $\mathbf{t}=\mathbf{R}_n+\boldsymbol{\tau}$, with $\mathbf{R}_n$ being a lattice vector and $\boldsymbol{\tau}$ being a fractional translation smaller than any lattice vector. The change of symmetry means that either some of the point-symmetry operations disappear or the translational vectors change.

If all the fractional translations τ_i's in a space group equal zero, that space group is known as symmorphic space group. For the unstrained and coherently strained

TABLE II. Deformation potentials used in linear deformation-potential calculation.

Deformation potential	Si	Ge
$(\Xi_d+\frac{1}{3}\Xi_u+a)_\Delta$	1.5[a]	1.31[b]
$(\Xi_d+\frac{1}{3}\Xi_u+a)_L$	−3.12[b]	−2.78[b]
Ξ_u^X	9.20[c]	9.42[c]
Ξ_u^L	16.14[b]	16.2[c]
D_μ	2.04[d]	3.32[e]
D'_μ	2.68[d]	3.81[e]

[a] Reference 27.
[b] Reference 18.
[c] Reference 25.
[d] Reference 26.
[e] Reference 28.

diamond structures, not all of the fractional translations τ_i's in the corresponding space group are zero, and thus the space groups discussed here are nonsymmorphic.

It is well known that the diamond structure has 48 point-symmetry operations and the space group is $O_h^7(Fd\bar{3}m)$. When Si and Ge are coherently grown on (001)-oriented $Si_{1-x}Ge_x$ substrates, some of the symmetry operations of the diamond structure no longer hold. For instance, the symmetry of all the threefold rotations ($\delta_{3xyz},\delta_{3xyz}^{-1}$, etc.) and reflections ($I\delta_{3xyz},I\delta_{3xyz}^{-1}$, etc.) are destroyed. On the other hand, the fractional translation τ changes from that of the diamond structure $\tau=(1,1,1)a_0/4$ to $\tau_1=(a,a,c)/4$, where a_0 is the lattice constant of the unstrained diamond structure, and a and c are the lattice constants of the [001] distorted diamond structure in the growth plane and in the growth direction, respectively. The space group of the distorted lattice becomes $D_{4h}^{19}(I4_1/amd)$ (Ref. 31) for the [001] growth case.

Similarly, for Si and Ge grown on (111)-oriented substrates, there are only 12 point-symmetry operations remaining, which are the identity and inversion symmetry, the threefold rotations and reflections along the [111] directions ($\delta_{3xyz},\delta_{3xyz}^{-1},I\delta_{3xyz},I\delta_{3xyz}^{-1}$), and the twofold rotations and reflections ($\delta_{2x\bar{y}},\delta_{2x\bar{z}},\delta_{2y\bar{z}},I\delta_{2x\bar{y}},I\delta_{2x\bar{z}},I\delta_{2y\bar{z}}$). These symmetry operations together with the new translation symmetry form a space group $D_{3d}^5(R\bar{3}m)$.[31] For Si and Ge grown on (110)-oriented substrates, none of the fourfold and threefold rotations and reflections are legitimate symmetry operations. Only eight point-symmetry operations—$E,I,\delta_{2z},\delta_{2xy},\delta_{2x\bar{y}},I\delta_{2z},I\delta_{2xy},I\delta_{2x\bar{y}}$—remain and the resulting space group is $D_{2h}^{28}(Imma)$.[31] The general symmetry properties for the three growth directions are listed in Table III.

Including the spin of an electron, we have the double space group G^D, doubling the numbers of symmetry elements:

$$G_{\text{space}}^D=[\{E|0\},\{|\bar{E}|0\},\{\alpha_2|\tau_2\},\{\bar{\alpha}_2|\tau_2\},\ldots,\{\alpha_g|\tau_g\},\{\bar{\alpha}_g|\tau_g\}]T\ , \tag{10}$$

where $\bar{E}$ corresponds to a 2π rotation of the spinor.

When the space group of the distorted diamond structure is known, the irreducible representations of the space group at any **k** point of the distorted Brillouin zone can be obtained. For example, when **k** is inside the first Brillouin zone, the irreducible representations of the group of **k** can be obtained by multiplying a factor $e^{-i\mathbf{k}\cdot\tau}$ to the irreducible representations of the corresponding point group. When **k** is on the surface of the first Brillouin zone, the procedure is complicated for nonsymmorphic space groups. Fortunately, the problem has already been solved.[32–35] Miller and Love,[36] and Bradley and Cracknell[20] have listed all the irreducible representations of the 230 space groups. Since spin-orbit splitting is included in the present calculation, the irreducible representations of the double space groups are used to denote all the energy bands throughout this paper. The symmetry properties of the $Si_{1-x}Ge_x$ alloy were analyzed by treating the random alloy as a virtual crystal.

The group of **k** along a symmetry line must be a subgroup of a special point of that line. Therefore, the irreducible representations at the symmetry point can be decomposed into a number of irreducible representations of the group of **k** along the symmetry line. Thus the compatibility relations between the bands of symmetry points and those of symmetry lines can be established. By analyzing the compatibility relations, the connections between the energy bands of the symmetry points and symmetry lines can be worked out. In this paper, the connection between all the energy bands for the [001], [111], and [110] growth cases have been confirmed with the compatibility relations.

In addition to the space-group symmetry operations, the Hamiltonian of an isolated crystal exhibits time-reversal symmetry. For example, for spinless particles, $H(\mathbf{r},-\mathbf{p})=H(\mathbf{r},\mathbf{p})$. Therefore, an additional degeneracy among eigenvalues may be expected. The judgment of whether additional degeneracy occurs or not is given by the Kramers theorem[37] and Wigner's rule.[38] Using that rule, we obtained information about additional degeneracies for the [001], [111], and [110] growth cases when time-reversal symmetry is included. The degeneracies due to time-reversal symmetry are denoted by the sum of two representations in the band-structure figures in this paper. Time-reversal symmetry may not apply if the system being considered is not isolated, for instance, in the presence of an electrical or magnetic field.

IV. BAND STRUCTURE AND SYMMETRY ANALYSIS

In this part the band-edge dependence of coherently grown $Si_{1-x}Ge_x$ alloys on the Ge content of both the epilayer and the substrate are discussed for different growth directions. The band-edge values are taken relative to the valence-band maximum of the substrate. Band offsets are obtained by linear interpolation of those of strained Si and Ge given by Van de Walle and Martin.[18] The calculation results are compared with those of linear deformation-potential theory.[25,26] By linear deformation potential we mean that constant deformation-potential values are used throughout the strain range and nonlinear effects such as the interaction between the conduction or valence bands are neglected. The band structures of coherently grown $Si_{1-x}Ge_x$ alloys along high-symmetry lines of the distorted Brillouin zone are analyzed together with the symmetry properties. The energy bands are either shifted (with no change of irreducible representations) or split (with new irreducible representations) from those of unstrained diamond structure.

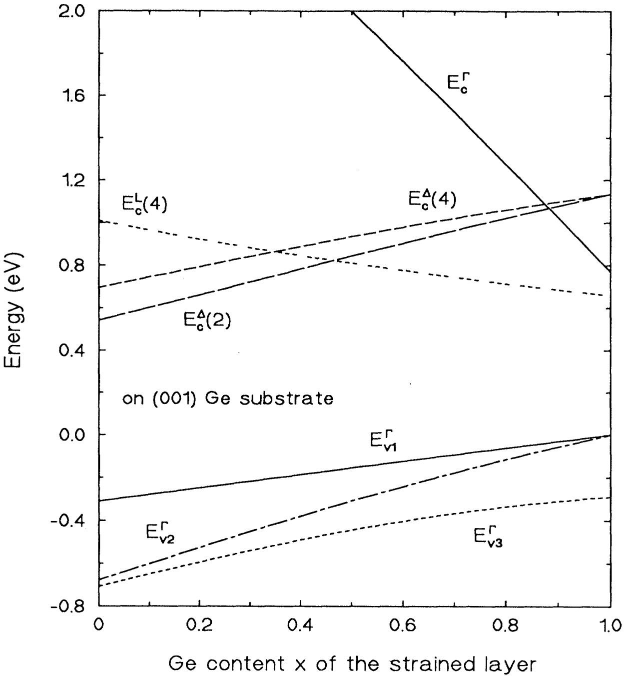

FIG. 7. Valence- and conduction-band-edge variations with Ge content x of coherently strained $Si_{1-x}Ge_x$ alloys grown on a (001) Ge substrate. Energy values are relative to the unstrained Ge substrate, and the band offsets are derived similarly to Fig. 6.

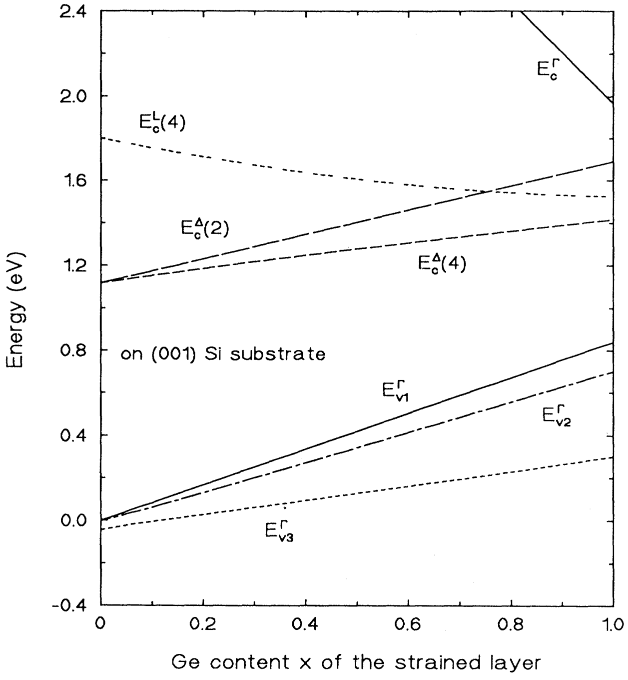

FIG. 6. Valence- and conduction-band-edge variations with Ge content x of coherently strained $Si_{1-x}Ge_x$ alloys grown on a (001) Si substrate. Energy values are relative to the unstrained Si substrate, and the band offsets are obtained from linear interpolation of strained Si and Ge given in Ref. 18.

A. [001] growth

Figures 6 and 7 show the band-edge variations of $Si_{1-x}Ge_x$ alloys grown on (001)-oriented Si and Ge substrates, respectively. One can see that the unstrained conduction-band minimum $E_c^\Delta(6)$ in the $\langle 100 \rangle$ directions of Figs. 1 and 2 is split into two values: $E_c^\Delta(2)$ and $E_c^\Delta(4)$ in Figs. 6 and 7. For strained alloys grown on (001) Si substrates shown in Fig. 6, $E_c^\Delta(4)$ in the growth plane are the conduction-band minima, and the fundamental band gaps decrease with increasing Ge content of the epilayer due to the increase of E_{v1}^Γ. For strained $Si_{1-x}Ge_x$ alloys grown on (001) Ge substrates, as shown in Fig. 7, the conduction-band minima change from $E_c^L(4)$ at the L point for Ge-rich alloys to $E_c^\Delta(2)$ in the [001] growth direction when the Ge content is below 0.6. Therefore, for Si-rich alloys grown on a (001) Ge substrate, $E_c^\Delta(2)$ in the [001] growth direction is the lowest conduction band. These results are in good agreement with those of linear deformation-potential theories.

Figures 8 and 9 show the band structures of Si grown on a (001)-oriented Ge substrate and Ge grown on a (001)-oriented Si substrate, respectively. At the Γ point of both figures, the two highest valence bands, Γ_6^+ ($|\frac{3}{2},\pm\frac{3}{2}\rangle$, heavy-hole band) and Γ_7^+ ($|\frac{3}{2},\pm\frac{1}{2}\rangle$, light-hole band), originate from the fourfold degenerate valence I_8^+ band of the unstrained diamond structure. Due to the opposite strains, the light-hole band Γ_7^+ is the top valence band for Si grown on a (001) Ge substrate, while the heavy-hole band Γ_6^+ is the top valence band for Ge grown on a (001) Si substrate. In Fig. 8, the energy difference of the light-hole band Γ_7^+ and heavy-hole band Γ_6^+ is much larger than that of the heavy-hole band Γ_6^+ and the spin-orbit split band Γ_7^+. The result here is in agreement with that of deformation-potential theory,[5] where the light-hole band $|\frac{3}{2},\pm\frac{1}{2}\rangle$ has an interaction with the spin-orbit splitting band $|\frac{1}{2},\pm\frac{1}{2}\rangle$ while the heavy-hole band $|\frac{3}{2},\pm\frac{3}{2}\rangle$ does not. By the same token, the light-hole band $|\frac{3}{2},\pm\frac{1}{2}\rangle$ (Γ_7^+) has a large separation from the spin-orbit splitting band $|\frac{1}{2},\pm\frac{1}{2}\rangle$ (in the lower Γ_7^+ band) in Fig. 9.

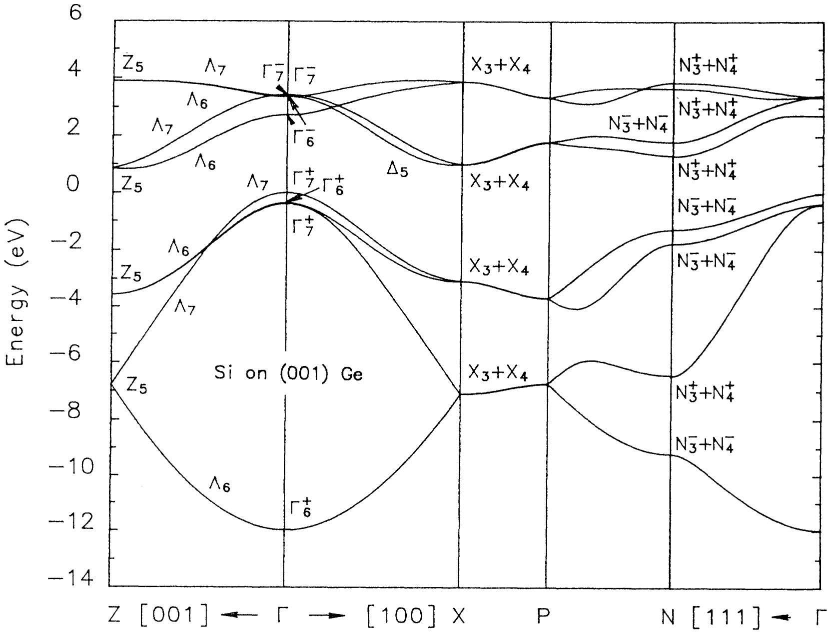

FIG. 8. The band structure of coherently strained Si grown on a (001) Ge substrate, along different directions of the distorted Brillouin zone. All the energy bands along the [100] direction are denoted by Δ_5.

For the [001] growth case, the symmetry along the [001] direction is not reduced, while the symmetry along the [100] and other directions is reduced by strain. Therefore the group of **k** along the [001] direction (line Λ and point Z) and the pertinent irreducible representations, Λ_6,Λ_7,Z_5, in Figs. 8 and 9 are the same as Δ_6,Δ_7,X_5 of an unstrained diamond structure [see Fig. 5(b)]. But the group of **k** along the [100] direction is changed and there is only one irreducible representation Δ_5 to denote all the energy bands in that direction (see Figs. 8 and 9). Therefore, all the bands at the Γ point connect with bands in the [100] direction with the Δ_5 representation. In contrast, for the [001] direction, two irreducible representations Λ_6 and Λ_7 exist, in which Λ_6 can connect with Γ_6^+ or Γ_6^-, and Λ_7 can connect with Γ_7^+ or Γ_7^-. From the irreducible representations, one can see that, along the [100] direction, no matter how closely some of the energy bands appear to approach each other, they actually do not cross, while Λ_6 and Λ_7 in the [001] direction can cross each other. Although the symmetry along the [100] direction is reduced, the four-degree degeneracy at the X point of the unstrained diamond structure is not lifted (including the degeneracy of X_3+X_4 due to time-reversal symmetry). The energy bands with irreducible representation X_3+X_4 are, however, different from X_5 of the unstrained diamond structure.

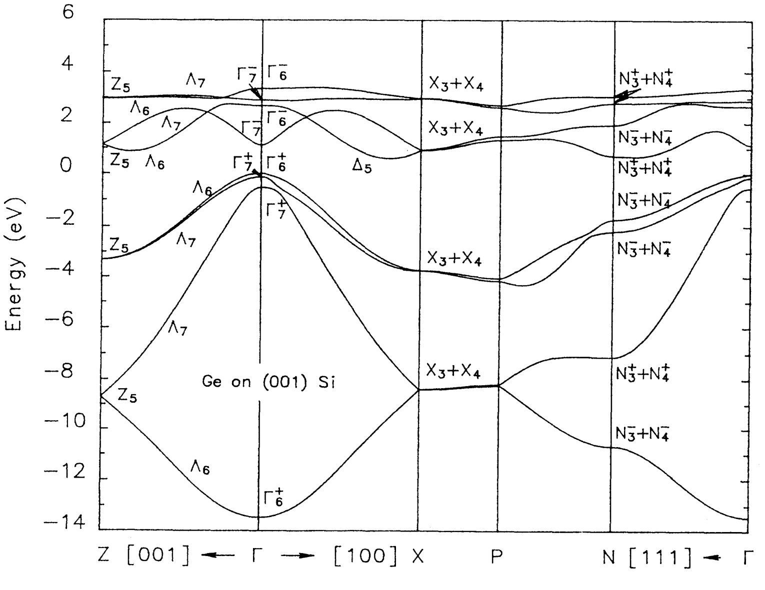

FIG. 9. The band structure of coherently strained Ge grown on a (001) Si substrate, along different directions of the distorted Brillouin zone. All the energy bands along the [100] direction are denoted by Δ_5.

TABLE III. Comparison of the symmetries of coherently strained diamond structures grown on (001)-, (111)-, and (110)-oriented substrates. a and c are the lattice constants in the growth plane and along the growth direction, respectively, for the [001] growth case; u_1 and u_3 are constants related to strain tensors, and their values are different for the [111] and [110] growth directions.

	Bulk Si and Ge	Bulk Si and Ge on (001) substrate	Bulk Si and Ge on (111) substrate	Bulk Si and Ge on (110) substrate
no. of point symmetry operations	48	16	12	8
space group	$Fd\bar{3}m(O_h^7)$	$I4_1/amd(D_{4h}^{19})$	$R\bar{3}m(D_{3d}^5)$	$Imma(D_{2h}^{28})$
Bravais lattice	body-centered cubic (Γ_c^v)	body-centered tetragonal (Γ_q^v)	trigonal (Γ_{rh})	body-centered orthorhombic (Γ_o^v)
fractional translation	$(1,1,1)a_0/4$	$(a,a,c)/4$	$u_1(1,1,1)a_0/4$	$(u_1,u_1,u_3)a_0/4$

It is important to note that the labels of the irreducible representations are only pertinent to their own space groups. For instance, Γ_6^+ of the unstrained diamond structure is an irreducible representation of group O_h^7, while Γ_6^+ of the [001] growth case is an irreducible representation of group D_{4h}^{19}. The relation between the irreducible representations of the unstrained and strained diamond structures are given in Table IV, which shows how the energy bands split from the unstrained diamond structure into those of the strained ones. For example, at the Γ point of Si grown on a (001)-oriented Ge substrate, the top valence band Γ_8^+ in Fig. 1 is split into two bands, Γ_6^+ and Γ_7^+ of Fig. 8, and the bottom conduction band Γ_8^- is split into Γ_6^- and Γ_7^-, while the Γ_6^+, Γ_7^+, Γ_6^-, Γ_7^- bands do not split.

B. [111] growth

The band-edge variations of $\mathrm{Si}_{1-x}\mathrm{Ge}_x$ alloys grown on a (111)-oriented Si substrate are shown in Fig. 10. The compressive stress of the strained layer lifts the conduction band at the L point and lowers the conduction band along the Δ line, making $E_c^{\Delta}(6)$ in the $\langle 100\rangle$ directions the lowest conduction band until $x \doteq 0.96$, beyond which the energy of $E_c^{\Delta}(6)$ and $E_c^{L2}(3)$ in the growth plane are very close each other. For $x > 0.96$, intervalley scattering between electrons in the L and Δ valleys may have some effect on the transport properties of the strained alloy. For $\mathrm{Si}_{1-x}\mathrm{Ge}_x$ alloys grown on (111) Ge substrates (see Ref. 39), $E_c^{L1}(1)$ in the [111] growth direction is the conduction-band minimum except for the $x<0.12$ region, where $E_c^{\Delta}(6)$ is shown to decrease rapidly with decreasing Ge content of the strained layer, falling below $E_c^{L1}(1)$ and becoming the lowest conduction band. This phenomenon differs from that of the linear deformation-potential formula,[25] where $E_c^{\Delta}(6)$ linearly increases with decreasing Ge content of the strained layer as discussed in Ref. 39. In the present calculation, for strained Si grown on (111) $\mathrm{Si}_{1-y}\mathrm{Ge}_y$ substrates, however, $E_c^{\Delta}(6)$ is always the lowest conduction band (also not shown). For strained Ge grown on (111) $\mathrm{Si}_{1-y}\mathrm{Ge}_y$ substrates, $E_c^{L2}(3)$ in the growth plane is always the lowest conduction band.

Figure 11 shows the band structure of strained Ge grown on a (111) Si substrate. At the Γ point, the two highest valence bands $\Gamma_4^+ + \Gamma_5^+$ and Γ_6^+ originate from Γ_8^+ of the unstrained Ge (Fig. 2). The heavy-hole band $|\frac{3}{2},\pm\frac{3}{2}\rangle$ $(\Gamma_4^+ + \Gamma_5^+)$ is the top valence band, which is opposite to the case of Si grown on a (111) Ge substrate, where the light hole $|\frac{3}{2},\pm\frac{1}{2}\rangle$ (Γ_6^+) is the top valence band (refer to Ref. 39). For Ge grown on a (111) Si substrate, the energy distance between the light-hole band Γ_6^+ and the spin-orbit split band $|\frac{1}{2},\pm\frac{1}{2}\rangle$ (Γ_6^+) is much larger than that of the heavy-hole band $|\frac{3}{2},\pm\frac{3}{2}\rangle$ $(\Gamma_4^+ + \Gamma_5^+)$ and the light-hole band Γ_6^+. This phenomenon is similar to that of the [001] growth case previously discussed.

For the [111] growth case, the symmetry along the [111] direction is not reduced, while the symmetry along the $[1\bar{1}1]$ and other directions is reduced. Therefore, the group of **k** along the [111] direction (line Λ and point Z)

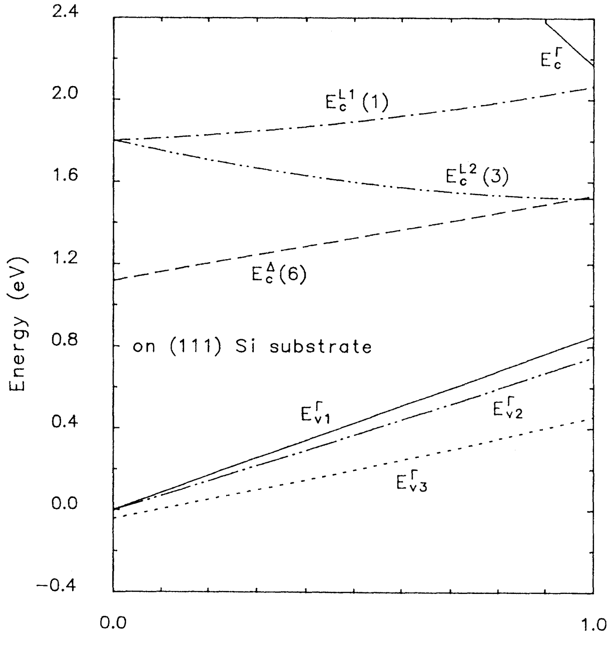

FIG. 10. Valence- and conduction-band-edge variations with Ge content x of the coherently strained $\mathrm{Si}_{1-x}\mathrm{Ge}_x$ alloy grown on a (111) Si substrate. Energy values are relative to the unstrained Si substrate, and the band offsets are derived similarly to Fig. 6.

TABLE IV. Decomposition of the irreducible representations at high-symmetry points and lines of the first Brillouin zone of unstrained diamond structure into those of coherently strained diamond structures grown on (001)-, (111)-, and (110)-oriented substrates.

(a) Decomposition into [001] strained structure (double group)

point Γ	Γ_6^+		Γ_7^+		Γ_8^+		Γ_6^-		Γ_7^-		Γ_8^-
$=>\Gamma$	Γ_6^+		Γ_7^+		$\Gamma_6^+ + \Gamma_7^+$		Γ_6^-		Γ_7^-		$\Gamma_6^- + \Gamma_7^-$
point X						X_5					
$=>X$						$X_3 + X_4$					
point X						X_5					
$=>Z$						Z_5					
point L	L_4^+		L_5^+		L_6^+		L_4^-		L_5^-		L_6^-
$=>N$	N_3^+		N_4^+		$N_3^+ + N_4^+$		N_4^-		N_3^-		$N_3^- + N_4^-$
point W		W_3			W_4		W_5		W_6		W_7
$=>P$		P_3			P_4		P_5		P_6		P_7
line Δ				Δ_6						Δ_7	
$=>\Delta$				Δ_5						Δ_5	
line Δ				Δ_6						Δ_7	
$=>\Lambda$				Λ_6						Λ_7	
line Σ						Σ_5					
$=>\Sigma$						Σ_5					
line S						S_5					
$=>F$						F_5					
line Z		Z_2			Z_3			Z_4			Z_5
$=>Y$		Y_2			Y_3			Y_4			Y_5
line Z		Z_2			Z_3			Z_4			Z_5
$=>W$		W_2			W_3			W_4			W_5
line Z		Z_2			Z_3			Z_4			Z_5
$=>U$		U_2			U_3			U_4			U_5
line Q				Q_3						Q_4	
$=>Q$				Q_3						Q_4	

(b) Decomposition into [111] strained structure (double group)

point Γ	Γ_6^+		Γ_7^+		Γ_8^+		Γ_6^-		Γ_7^-		Γ_8^-
$=>\Gamma$	Γ_6^+		Γ_6^+		$\Gamma_4^+ + \Gamma_5^+ + \Gamma_6^+$		Γ_6^-		Γ_6^-		$\Gamma_4^- + \Gamma_5^- + \Gamma_6^-$
point X						X_5					
$=>F$						$F_3^+ + F_4^+ + F_3^- + F_4^-$					
point L	L_4^+		L_5^+		L_6^+		L_4^-		L_5^-		L_6^-
$=>L$	L_3^+		L_4^+		$L_3^+ + L_4^+$		L_4^-		L_3^-		$L_3^- + L_4^-$
point L	L_4^+		L_5^+		L_6^+		L_4^-		L_5^-		L_6^-
$=>Z$	Z_4^+		Z_5^+		Z_6^+		Z_4^-		Z_5^-		Z_6^-
line Λ		Λ_4			Λ_5						Λ_6
$=>\Lambda$		Λ_4			Λ_5						Λ_6
line Σ						Σ_5					
$=>\Sigma$						$\Sigma_3 + \Sigma_4$					
line S						S_5					
$=>Q$						$Q_3 + Q_4$					
line Q				Q_3						Q_4	
$=>B$				B_3						B_4	
line Q				Q_3						Q_4	
$=>Y$				Y_3						Y_4	

(c) Decomposition into [110] strained structure (double group)

point Γ	Γ_6^+		Γ_7^+		Γ_8^+		Γ_6^-		Γ_7^-		Γ_8^-
$=>\Gamma$	Γ_5^+		Γ_5^+		$\Gamma_5^+ + \Gamma_5^+$		Γ_5^-		Γ_5^-		$\Gamma_5^- + \Gamma_5^-$
point X						X_5					
$=>T$						$T_2 + T_2$					
point L	L_4^+		L_5^+		L_6^+		L_4^-		L_5^-		L_6^-
$=>R$	R_3^+		R_4^+		$R_3^+ + R_4^+$		R_4^-		R_3^-		$R_3^- + R_4^-$
point L	L_4^+		L_5^+		L_6^+		L_4^-		L_5^-		L_6^-
$=>S$	S_3^+		S_4^+		$S_3^+ + S_4^+$		S_4^-		s_3^-		$S_3^- + S_4^-$
point W		W_3			W_4		W_5		W_6		W_7
$=>W$		W_2			W_4		W_2		W_4		$W_3 + W_5$
line Δ				Δ_6						Δ_7	

TABLE IV. (*Continued*).

	(c) Decomposition into [110] strained structure (double group)								
$=>\Lambda$		Λ_5					Λ_5		
line Σ					Σ_5				
$=>\Sigma$					Σ_5				
line Σ					Σ_5				
$=>\Delta$					Δ_5				
line S					S_5				
$=>F$					F_5				
line S					S_5				
$=>U$					U_5				
line Z	Z_2			Z_3		Z_4			Z_5
$=>P$	P_4			P_3		P_3			P_4
line Q			Q_3					Q_4	
$=>Q$			Q_3					Q_4	
line Q			Q_3					Q_4	
$=>D$			D_3					D_4	

and the pertinent irreducible representations are the same as those of an unstrained diamond structure (line Λ and point L of Figs. 1 and 2), while the group of **k** and the irreducible representations along the $[1\bar{1}1]$ direction are changed. Although the symmetry along the six $\langle 100 \rangle$ directions remains equivalent, this symmetry is reduced and is lower than that of an unstrained diamond structure. Thus the four-degree degenerate state X_5 is split into two bands $F_3^+ + F_4^+$ and $F_3^- + F_4^-$ with even and odd parities, respectively. The degeneracy of F_3^+ and F_4^+ is due to time-reversal symmetry, as is the case for F_3^- and F_4^-. (A representation is said to have an even or odd parity when its character under the inversion symmetry operation is the same as or negative to, respectively, that of the identity operation.) The stress-induced splitting of the X_5 state into the pair $F_3^+ + F_4^+$ and $F_3^- + F_4^-$ exhibits nonlinearity and this splitting increases very fast with increasing strain. This effect is automatically included in our calculation but not explicitly considered in the linear deformation-potential calculation formula given in Refs. 5 and 25.

For $Si_{1-x}Ge_x$ alloys coherently grown on (111) Si substrates, when the Ge content of the strained layer increases from 0.0 to 1.0, the volume compression makes the center of the two lowest conduction bands $F_3^+ + F_4^+$ and $F_3^- + F_4^-$ of Fig. 11, for example, lower with increasing strain. The nonlinear splitting between the $F_3^+ + F_4^+$ and $F_3^- + F_4^-$ bands also makes the $F_3^- + F_4^-$ band move further down. Therefore, the band-edge variation with Ge content of the strained $Si_{1-x}Ge_x$ alloys has the same trend in our calculation as those of the linear deformation-potential formula. But, for $Si_{1-x}Ge_x$ alloys coherently grown on (111) Ge substrates (again not shown here, but discussed in Ref. 39), the volume expansion and the nonlinear splitting have different effects on the lowest conduction band $F_3^+ + F_4^+$ at the F point.

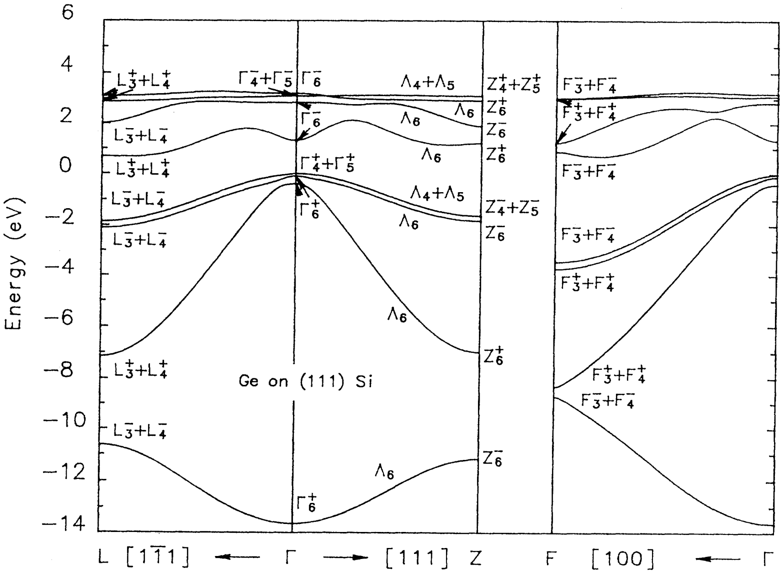

FIG. 11. The band structure of coherently strained Ge grown on a (111) Si substrate, along different directions of the distorted Brillouin zone.

Since the nonlinear splitting increases faster with strain, the lowest $F_3^+ + F_4^+$ conduction band [$E_c^\Delta(6)$] goes lower for large strain. The lifting of the conduction-band degeneracy at the point X of bulk Si under stress has been previously evidenced in several experiments.[40,41,27] The nonlinear splittings in the experimental results have been explained by Hensel, Hasegawa, and Nakayama, and Laude, Pollak, and Cardona, and they have added a splitting parameter Ξ_u' or ε_2^*, a new shear deformation potential, to account for this splitting. A discussion of nonlinear splittings and the comparison between the results of the present calculation and Hensel's model is given in Ref. 39.

C. [110] growth

The band-edge variations of $Si_{1-x}Ge_x$ alloys grown on (110)-oriented Si and Ge substrates are shown in Figs. 12 and 13, respectively. For $Si_{1-x}Ge_x$ alloys grown on (110) Si substrates, shown in Fig. 12, the conduction-band minima are $E_c^\Delta(2)$ along the [001] direction for almost all Ge contents except the $x > 0.96$ region, where the energies of $E_c^\Delta(2)$ and $E_c^{L2}(2)$ in the [$\bar{1}$11] direction are very close. Therefore, near the band crossover point ($x \doteq 0.96$), intervalley scattering between the L and the Δ valleys is possible for $Si_{1-x}Ge_x$ alloys grown on a (110) Si substrate. For $Si_{1-x}Ge_x$ alloys grown on (110) Ge substrates, as shown in Fig. 13, the conduction-band minimum changes from $E_c^{L2}(2)$ in the [1$\bar{1}$1] direction into $E_c^\Delta(2)$ in the [001] direction as the Ge content decreases to below 0.4. However, the linear deformation-potential formula used in Refs. 25 and 5 always give $E_c^\Delta(2)$, being higher than $E_c^\Delta(4)$ for all Ge contents.

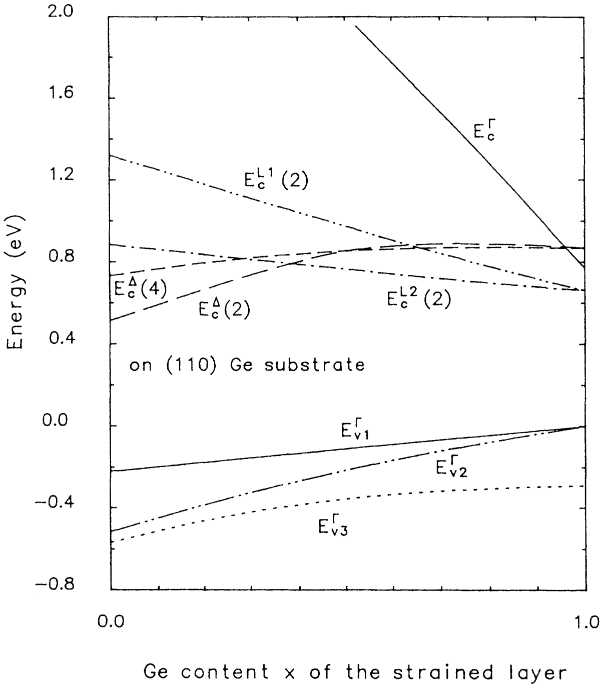

FIG. 13. Valence- and conduction-band-edge variations with Ge content x of the coherently strained $Si_{1-x}Ge_x$ alloy grown on a (110) Ge substrate. Energy values are relative to the unstrained Ge substrate, and the band offsets are derived similarly to Fig. 6.

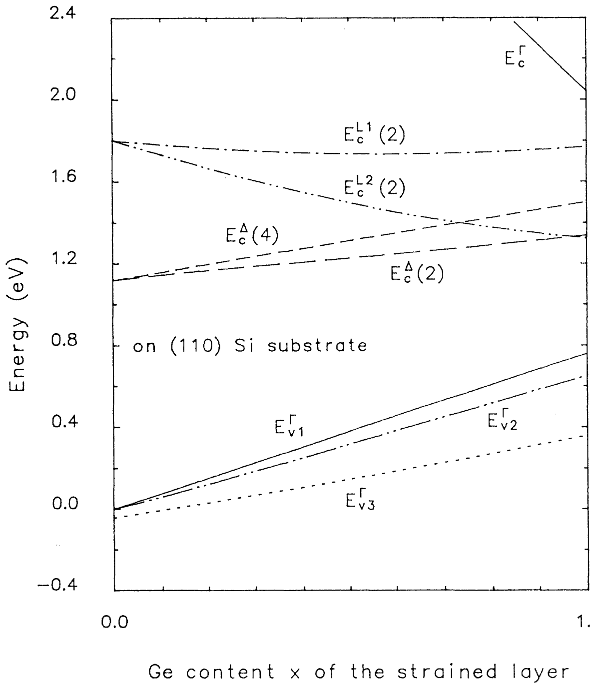

FIG. 12. Valence- and conduction-band-edge variations with Ge content x of the coherently strained $Si_{1-x}Ge_x$ alloy grown on a (110) Si substrate. Energy values are relative to the unstrained Si substrate, and the band offsets are derived similarly to Fig. 6.

Figures 14 and 15 show the band structures of strained Si grown on a (110) Ge substrate and strained Ge grown on a (110) Si substrate, respectively. In this case, the [110] and [1$\bar{1}$0] directions are no longer equivalent but their symmetry remains unchanged by the strain. Thus the irreducible representations along the [110] and [1$\bar{1}$0] directions are the same as those of an unstrained diamond structure, while the energy-band structures in these two directions differ from each other as shown in Figs. 14 and 15. The symmetries at the Γ point and along the [100], [001], [111], and [1$\bar{1}$1] directions are all reduced, resulting in different energy bands. At the Γ point, the conduction bands are all Γ_5^-, while all the valence bands are Γ_5^+, where both the Γ_5^+ and Γ_5^- are two-degree degenerate. The fourfold-degenerate X_5 state of unstrained Si is split into two T_2 states at the T point, and into the X_5^+ and X_5^- states at point X. It is interesting to note that the splitting between the X_5^+ and X_5^- states, which are of the even and odd parities, respectively, is much larger than that of the two T_2 states, the latter of which is too small to be seen in the figure. It can be seen that for the [110] growth case, the band structures along the [100] and [001] directions are different due to the symmetry reduction by the strain, as are the band structures in the [111] and [1$\bar{1}$1] directions (see Figs. 14 and 15). The

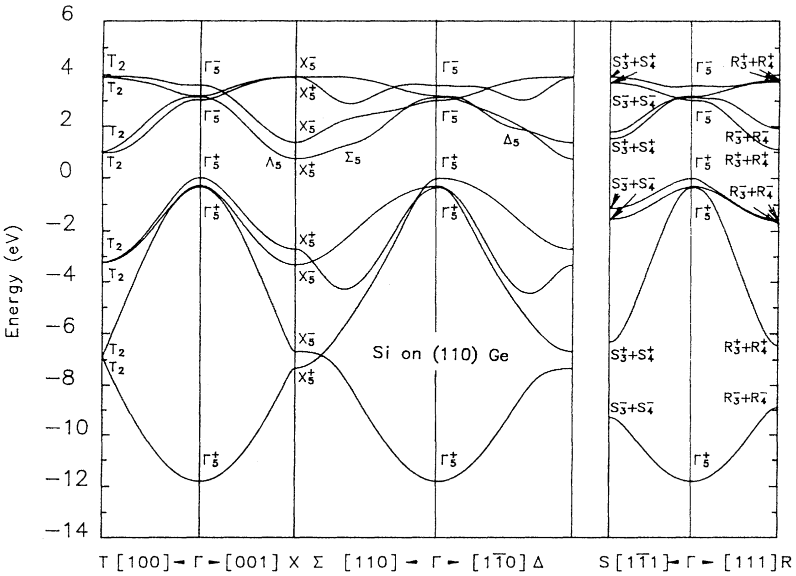

FIG. 14. The band structure of coherently strained Si grown on a (110) Ge substrate, along different directions of the distorted Brillouin zone. Since there is only one irreducible representation to denote all the energy bands along the [001], [110], and [1$\bar{1}$0] directions, respectively, only one symbol is shown for each of the three directions.

nonequivalence of the band structures in the [100] and [001], [111] and [1$\bar{1}$1], and [110] and [1$\bar{1}$0] directions give different effective masses of the heavy and light holes, which are indicated clearly by the significant differences in the valence-band curvatures.

Similar to the F point in the [111] growth case described previously, the splitting of the X_5 state into a pair of X_5^+ and X_5^- bands for the [110] growth is a nonlinear effect, which increases rapidly with the strain. For $\mathrm{Si}_{1-x}\mathrm{Ge}_x$ alloys grown on (110) Si substrates, similar to the case of Fig. 15, the nonlinear splitting of the X_5^+ and X_5^- states and the volume compression both make the X_5^- conduction state decrease with increasing Ge content of the alloy. But for $\mathrm{Si}_{1-x}\mathrm{Ge}_x$ alloys grown on (110) Ge substrates, the nonlinear splitting of the X_5^+ and X_5^- states has an opposite effect on the X_5^+ band compared with that of volume expansion, thus resulting in $E_c^\Delta(2)$ decreasing as shown in Fig. 13. The nonlinear band-edge splitting is discussed in Ref. 39.

It can be known that there is a point K in the [110] direction of the second Brillouin zone which is equivalent to point X in the $\langle 100 \rangle$ directions of the unstrained diamond structure, shown in Figs. 1 and 2. For $\mathrm{Si}_{1-x}\mathrm{Ge}_x$ alloys coherently grown on (110)-oriented substrates, the point K in the [110] direction of the second Brillouin zone is equivalent to point X in the [001] direction but not to point T in the [100] direction. Therefore, whenever $E_c^\Delta(2)$ in the [001] direction is the conduction-band minimum, that minimum also exists in the [110] direction of the second Brillouin zone. This phenomenon is due to the following relation:

$$\mathbf{k}_{[110],K} = \mathbf{k}_{[001],X} + \mathbf{K}_h \ , \tag{11}$$

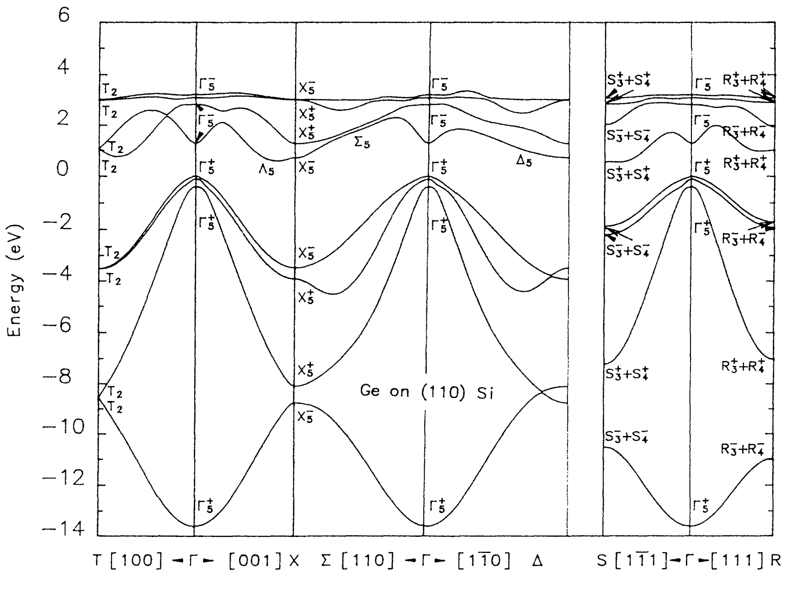

FIG. 15. The band structure of coherently strained Ge grown on a (110) Si substrate, along different directions of the distorted Brillouin zone. Since there is only one irreducible representation to denote all the energy bands along the [001], [110], and [1$\bar{1}$0] directions, respectively, only one symbol is shown for each of the three directions.

$$\mathbf{k}_{[110],K} \neq \mathbf{k}_{[100],Z} + \mathbf{K}_h \ , \tag{12}$$

where $\mathbf{K}_h$ is a reciprocal vector of the distorted lattice. This phenomenon is favorable for optical transitions if zone folding is expected to occur in superlattice structures.

The even- and odd-parity characteristics of the energy bands in the [001], [111], and [110] growth cases are very interesting. If the original band in the unstrained diamond structure has an even or odd parity, the split or shifted bands under strain retain the same parity as the original one. For all three growth cases at the Γ point, all the valence bands have even parities, while all the conduction bands have odd parities. If the original band in the unstrained diamond structure does not have an even or odd parity, the split or shifted bands under strain either remain parityless or split into a pair of bands with an even and odd parity. This can be seen from Figs. 14 and 15 for the [110] growth case, where the X_5 band in the [100] direction is split into two parityless T_2 states, while in the [001] direction it is split into the X_5^+ and X_5^- pair. Furthermore, the relative position of the split bands with the even and odd parities will switch as the strain changes sign, i.e., expansion or compression. For example, at the X point of the [110] growth case, X_5^- is the lowest conduction band if the alloy is under compressive strain (Fig. 15), while X_5^+ becomes the lowest conduction band if the alloy is under tensile strain (Fig. 14). The splitting of a parityless band into a pair of even and odd bands is important in the sense that the interaction between the even and odd bands may be very large and the resulting effects of this splitting, such as band-edge variations and optical transitions, should not be neglected in large strain cases.

V. SELECTION RULES FOR DIRECT TRANSITIONS

Besides denoting the energy bands, the irreducible representations of a space group can also be used to determine selection rules for optical transitions. For simplicity, only direct transitions are discussed here.

For optical transitions, one must calculate the matrix elements of this type,

$$\langle \phi_m^{(\mathbf{k}_2,\mu)} | V | \psi_n^{(\mathbf{k}_1,\nu)} \rangle \ , \tag{13}$$

where V is the perturbation function, $\psi_n^{(\mathbf{k}_1,\nu)}$ ($n=1,2,3,\ldots,l_\nu$) is the initial state transforming as the irreducible representation $D^{(\mathbf{k}_1,\nu)}$ of the group of $\mathbf{k}_1$, $\phi_m^{(\mathbf{k}_2,\mu)}$ ($m=1,2,3,\ldots,l_\mu$) is the final state transforming as the irreducible representation $D^{(\mathbf{k}_2,\mu)}$ of the group of $\mathbf{k}_2$, and l_ν and l_μ are the dimensions of the two irreducible representations, respectively. For direct optical transitions, we have $\mathbf{k}_1 = \mathbf{k}_2$.

Suppose $D^{\beta}(\alpha_{\mathbf{k}_1})$ denotes the representation of the point group of $\mathbf{k}_1$ to which the perturbation function V belongs, the product function $V\psi_n^{(\mathbf{k}_1,\nu)}$ belongs to the product representation $D^{(\beta)}(\alpha_{\mathbf{k}_1}) \times D^{(\mathbf{k}_1,\nu)}(\{\alpha_{\mathbf{k}_1}|\tau\})$ of the group of $\mathbf{k}_1$. According to the orthogonal theorem of group theory, the number of times which the representation $D^{(\mathbf{k}_1,\mu)}$ appears in the above product representation is given by[42]

$$C(\mu,\beta,\nu) = \frac{1}{h_{\mathbf{k}_1}} \sum_{\{\alpha_{\mathbf{k}_1}|\tau\}} \chi^{(\mathbf{k}_1,\mu)}(\{\alpha_{\mathbf{k}_1}|\tau\}) \chi^{\beta}(\alpha_{\mathbf{k}_1}) \times \chi^{(\mathbf{k}_1,\nu)}(\{\alpha_{\mathbf{k}_1}|\tau\}) \ , \tag{14}$$

where $h_{\mathbf{k}_1}$ is the number of symmetry elements in the group of $\mathbf{k}_1$ and $\chi(\{\alpha_{\mathbf{k}_1}|\tau\})$ denotes the character of the irreducible representation for the symmetry operation $\{\alpha_{\mathbf{k}_1}|\tau\}$. The selection rules are obtained by determining whether or not the value $C(\mu,\beta,\nu)$ is equal to zero for forbidden and allowed transitions, respectively.

In the electric dipole approximation, the perturbation function V is proportional to $\mathbf{e}\cdot\mathbf{r}$, where $\mathbf{e}$ is the polarization vector of the radiation field. The selection rules for direct optical transitions at high-symmetry points and lines of the distorted Brillouin zones for the [001], [111], and [110] growth cases are illustrated in Table V. Shown in the first column of Table V are the irreducible representations of the perturbation and the pertinent basis functions. For every symmetry point or line, the irreducible representations of the group of $\mathbf{k}$ for the initial states are listed in the upper subrow. The next subrows, within boxes, give the irreducible representations of the final states that have nonvanishing matrix elements of Eq. (14).

By analyzing Table V and referring to the band structures in Figs. 8–15, the following conclusions can be obtained:

(1) At the same $\mathbf{k}$ point or line, if there is only one irreducible representation denoting all the energy bands, then the transitions between any two bands are allowed.

(2) Since the perturbation is the electric dipole approximation, $V \sim \mathbf{e}\cdot\mathbf{r}$, which is an odd function of space coordinates, transitions between two bands with the same parities are forbidden, while transitions between two bands with different parities may be allowed. At the Γ point, all the valence bands have even parities, while all the conduction bands have odd parities. Therefore, transitions between a valence band and a conduction band may be allowed, while transitions between two valence bands or between two conduction bands are forbidden.

(3) Selection rules may depend on the polarization of the incident light.

Figure 16 shows the selection rules for direct transitions at the Γ point of Ge grown on a (001)-oriented Si substrate. When the light is polarized parallel to the z ([001]) direction, only transitions between Γ_6^+ and Γ_6^-, and Γ_7^+ and Γ_7^- are allowed. When the light is polarized parallel to the growth plane (xy plane), all the transitions among the $\Gamma_6^+, \Gamma_7^+, \Gamma_6^-, \Gamma_7^-$ bands are allowed. From Table V, it can be seen that when light is polarized parallel to the growth direction, the transitions between Λ_6 and Λ_7 along the [001] growth direction are not allowed either. If polarized in the growth plane (such as along the [100] direction), transitions between any two bands are permitted, independent of the polarization of the incident light. The transitions between the lowest conduc-

TABLE V. Selection rules for direct optical transitions at high-symmetry points and lines for diamond structures coherently grown on (001), (111), and (110) substrates. The first column gives the dipole irreducible representations and the basis functions.

(a) [001] growth case (double group)

Point Γ	Γ_i	Γ_6^+	Γ_7^+	Γ_6^-		Γ_7^-
$\Gamma_2^-;z$	$\Gamma_i\times\Gamma_2^-$	Γ_6^-	Γ_7^-	Γ_6^+		Γ_7^+
$\Gamma_5^-;(x,y)$	$\Gamma_i\times\Gamma_5^-$	$\Gamma_6^-+\Gamma_7^-$	$\Gamma_6^-+\Gamma_7^-$	$\Gamma_6^++\Gamma_7^+$		$\Gamma_6^++\Gamma_7^+$
Point N	N_i	N_3^+	N_4^+	N_3^-		N_4^-
$N_1^-;x-y$	$N_i\times N_1^-$	N_3^-	N_4^-	N_3^+		N_4^+
$2N_2^-;x+y,z$	$N_i\times N_2^-$	N_4^-	N_3^-	N_4^+		N_3^+
Point X	X_i		X_3			X_4
$X_6^0;y$	$X_i\times X_6^0$		X_3			X_4
$X_7^0;z$	$X_i\times X_7^0$		X_3			X_4
$X_8^0;x$	$X_i\times X_8^0$		X_4			X_3
Point P	P_i	P_3	P_4	P_5	P_6	P_7
$P_2^0;z$	$P_i\times P_2^0$	P_6	P_5	P_4	P_3	P_7
$P_5^0;(x,y)$	$P_i\times P_5^0$	P_7	P_7	P_7	P_7	$P_3+P_4+P_5+P_6$
Line Λ	Λ_i		Λ_6			Λ_7
$\Lambda_1;z$	$\Lambda_i\times\Lambda_1$		Λ_6			Λ_7
$\Lambda_5;(x,y)$	$\Lambda_i\times\Lambda_5$		$\Lambda_6+\Lambda_7$			$\Lambda_6+\Lambda_7$
Line W	W_i	W_2	W_3	W_4	W_5	
$W_1^0;z$	$W_i\times W_1^0$	W_2	W_3	W_4	W_5	
$W_3^0;x$	$W_i\times W_3^0$	W_3	W_2	W_5	W_4	
$W_4^0;y$	$W_i\times W_4^0$	W_5	W_4	W_3	W_2	
Line Q	Q_i		Q_3			Q_4
$Q_1;x-y$	$Q_i\times Q_1$		Q_3			Q_4
$2Q_2;x+y,z$	$Q_i\times Q_2$		Q_4			Q_3

(b) [111] growth case (double group)

Point Γ,Z	Γ_i	Γ_4^+	Γ_5^+	Γ_6^+	Γ_4^-	Γ_5^-	Γ_6^-
$\Gamma_1^-;x+y+z$	$\Gamma_i\times\Gamma_1^-$	Γ_4^-	Γ_5^-	Γ_6^-	Γ_4^+	Γ_5^+	Γ_6^+
$\Gamma_3^-;[x+y-2z,\sqrt{3}(x-y)]$	$\Gamma_i\times\Gamma_3^-$	Γ_6^-	Γ_6^-	$\Gamma_4^-+\Gamma_5^-+\Gamma_6^-$	Γ_6^+	Γ_6^+	$\Gamma_4^++\Gamma_5^++\Gamma_6^+$
point L,F	L_i	L_3^+		L_4^+	L_3^-		L_4^-
$L_1^-;x-z$	$L_i\times L_1^-$	L_3^-		L_4^-	L_3^+		L_4^+
$2L_2^-;x+z,y$	$L_i\times L_2^-$	L_4^-		L_3^-	L_4^+		L_3^+
Line Λ	Λ_i	Λ_4		Λ_5			Λ_6
$\Lambda_1;x+y+z$	$\Lambda_i\times\Lambda_1$	Λ_4		Λ_5			Λ_6
$\Lambda_3;[\sqrt{3}(x-y),2z-x-y]$	$\Lambda_i\times\Lambda_3$	Λ_6		Λ_6			$\Lambda_4+\Lambda_5+\Lambda_6$
Line B,Σ,Q,Y	B_i		B_3				B_4
$B_1;x-y$	$B_i\times B_1$		B_3				B_4
$2B_2;x+y,z$	$B_i\times B_2$		B_4				B_3

(c) [110] growth case (double group)

Point Γ,X	Γ_i		Γ_5^+			Γ_5^-	
$\Gamma_2^-;x-y$	$\Gamma_i\times\Gamma_2^-$		Γ_5^-			Γ_5^+	
$\Gamma_3^-;z$	$\Gamma_i\times\Gamma_3^-$		Γ_5^-			Γ_5^+	
$\Gamma_4^-;x+y$	$\Gamma_i\times\Gamma_4^-$		Γ_5^-			Γ_5^+	
point R,S	R_i	R_3^+		R_4^+	R_3^-		R_4^-
$R_1^-;x-y$	$R_i\times R_1^-$	R_3^-		R_4^-	R_3^+		R_4^+
$2R_2^-;x+y,z$	$R_i\times R_2^-$	R_4^-		R_3^-	R_4^+		R_3^+
Point W	W_i	W_2		W_3	W_4		W_5
$W_2^0;z$	$W_i\times W_2^0$	W_4		W_5	W_2		W_3
$W_3^0;x-y$	$W_i\times W_3^0$	W_5		W_4	W_3		W_2
$W_4^0;x+y$	$W_i\times W_4^0$	W_3		W_2	W_5		W_4
Line P,Q	P_i		P_3			P_4	
$P_1;z$	$P_i\times P_1$		P_3			P_4	
$2P_2;x,y$	$P_i\times P_2$		P_4			P_3	
Line D	D_i		D_3			D_4	
$D_1;x+y$	$D_i\times D_1$		D_3			D_4	
$2D_2;x-y,z$	$D_i\times D_2$		D_4			D_3	

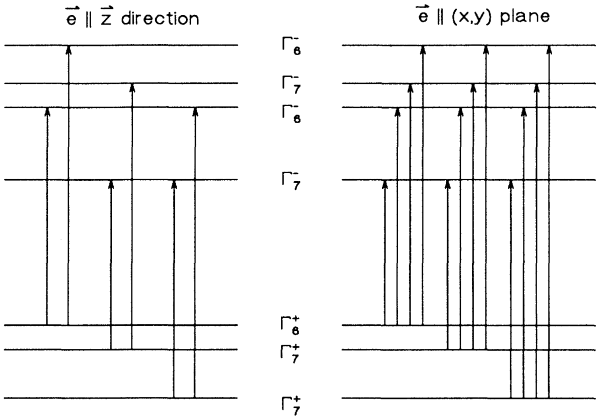

FIG. 16. Selection rules for direct transitions among energy bands at the Γ point of coherently strained Ge grown on a (001) Si substrate. **e** is the polarization vector of the incident light, **z** is the unit vector in the [001] growth direction.

tion band ($N_3^+ + N_4^+$) and the highest valence band ($N_3^- + N_4^-$) at point N are also allowed.

For the [111] growth case, the selection rules depend on the polarization direction at the Γ (and Z) point. For example, when light is polarized along the growth direction, the transitions between the $\Gamma_4^+ + \Gamma_5^+$ and $\Gamma_4^- + \Gamma_5^-$ are allowed. On the other hand, when light is polarized parallel to the growth plane, the transitions between $\Gamma_4^+ + \Gamma_5^+$ and Γ_6^- are allowed. At the L and F points, the selection rules have no dependence on the polarization direction of the incident light.

For the [110] growth case, direct transitions are independent of the polarization direction. At the Γ point, the transitions between Γ_5^+ and Γ_5^-, i.e., between any valence band and any conduction band, are allowed. At the X point, the minimum-energy transitions between X_5^+ and X_5^+, or X_5^- and X_5^-, are forbidden. At the points R and S, the transitions between $R_3^+ + R_4^+$ and $R_3^- + R_4^-$, $S_3^+ + S_4^+$ and $S_3^- + S_4^-$ are allowed. Along all the other high-symmetry lines, such as [100], [001], [111], [1$\bar{1}$1], [110], and [1$\bar{1}$0] directions, transitions between any two bands are allowed.

VI. SUMMARY

A semiempirical tight-binding method has been used to calculate the band structures of $\mathrm{Si}_{1-x}\mathrm{Ge}_x$ alloys coherently grown on (001)-, (111)-, and (110)-oriented $\mathrm{Si}_{1-y}\mathrm{Ge}_y$ substrates. Strain tensors were carefully studied for the three growth directions and the strain effect was incorporated in the geometrical factors and the integral parameters of the tight-binding formulas. The distorted crystal structures and the distorted Brillouin zones were shown. The band-edge variations of the $\mathrm{Si}_{1-x}\mathrm{Ge}_x$ alloys coherently grown on different $\mathrm{Si}_{1-y}\mathrm{Ge}_y$ substrates were obtained. The band structures and symmetry properties of the strained $\mathrm{Si}_{1-x}\mathrm{Ge}_x$ alloys along high-symmetry lines of the distorted Brillouin zone were analyzed in detail. The conduction-band valley $E_c^{\Delta}(6)$ in the ⟨100⟩ directions was split into two kinds of valleys: $E_c^{\Delta}(4)$ and $E_c^{\Delta}(2)$ for the [001] and [110] growth cases, while the conduction-band valley $E_c^{L}(4)$ in the ⟨111⟩ directions was split into two kinds of valleys: $E_c^{L1}(1)$ and $E_c^{L2}(3)$, or $E_c^{L1}(2)$ and $E_c^{L2}(2)$ for the [111] and [110] growth cases, respectively. For the [001] and [111] growth cases, the conduction-band minima appeared in the growth direction only when the epilayer was under a tensile strain, i.e., the unstrained lattice constant of the epilayer is smaller than that of the substrate. For the [111] and [110] growth cases, the four-degree degenerate state X_5 in the [001] direction of an unstrained diamond structure was split into two bands with even and odd parities, respectively, due to the symmetry reduction by the strain. It was found that the splitting between the two bands with even and odd parities was a nonlinear effect, which increased rapidly with increasing strain. The overall effect made the conduction-band edge $E_c^{\Delta}(6)$ for the [111] growth case and $E_c^{\Delta}(2)$ for the [110] growth case decrease with increasing strain for $\mathrm{Si}_{1-x}\mathrm{Ge}_x$ alloys grown on Ge substrates. These results deviated from those of linear deformation-potential theory, which did not explicitly consider the nonlinear effect.

The band structures in the present calculations are consistent with the compatibility relations between the irreducible representations of symmetry points and lines in the distorted Brillouin zones. The relations between the energy states of an unstrained diamond structure and those of strained ones were shown in the band-structure figures. Additional degeneracies due to time-reversal symmetry were also labeled for convenience of reference. Selection rules for direct optical transitions were given for the $\mathrm{Si}_{1-x}\mathrm{Ge}_x$ alloys coherently grown on the (001)-, (111)-, and (110)-oriented $\mathrm{Si}_{1-y}\mathrm{Ge}_y$ substrates using the electric-dipole approximation. The results showed that at the Γ point, transitions between a valence and a conduction band may be allowed, while transitions between two valence or two conduction bands are forbidden. In some cases, selection rules depend on the polarization of the incident light, in which case more transitions can be allowed when the light is polarized parallel to the growth plane.

ACKNOWLEDGMENTS

This work was partly supported by the U.S. Office of Naval Research (ONR) monitored by Dr. George Wright and Dr. Kristl Hathaway. The authors would like to sincerely thank Dr. G. and Dr. M. S. Dresselhaus for their helpful discussions and suggestions on group theory. One of us (Q.M.M.) is especially grateful for the help of Professor Jinsheng Luo of Xian Jiaotong University, China, in her early studies of this work.

[1] J. C. Bean, L. C. Feldman, A. T. Fiory, S. Nakahara, and I. K. Robinson, J. Vac. Sci. Technol. A **2**, 436 (1984).

[2] E. Kasper, H. Kibbel, H. Jorke, H. Brugger, E. Friess, and G. Abstreiter, Phys. Rev. B **38**, 3599 (1988).

[3] K. L. Wang, R. P. Karunasiri, J. Park, S. S. Rhee, and C. H. Chern, Superlatt. Microstruct. **5**, 201 (1989).

[4] R. P. G. Karunasiri, J. S. Park, K. L. Wang, and Li-Jen Cheng, Appl. Phys. Lett. **56**, 1342 (1990).

[5] R. People, Phys. Rev. B **32**, 1405 (1985).

[6] R. People and J. C. Bean, Appl. Phys. Lett. **39**, 538 (1986).

[7] D. J. Chadi, Phys. Rev. B **16**, 790 (1977).

[8] K. C. Hass, Phys. Rev. B **27**, 1088 (1983).

[9] J. C. Slater and G. F. Koster, Phys. Rev. **94**, 1498 (1954).

[10] D. Shen, F. Lu, K. Zhang, and X. Xie, Appl. Phys. Lett. **52**, 1599 (1988).

[11] J. R. Chelikowsky and M. L. Cohen, Phys. Rev. B **14**, 556 (1976).

[12] O. Madelung, M. Schulz, and H. Weiss, in *Numerical Data and Functional Relationships in Science and Technology,* edited by O. Madelung, Landolt-Börnstein, New Series, Group III, Vol. 17, Pt. 1.6 (Springer-Verlag, New York, 1982), pp. 449ff.

[13] M. Podgorny, G. Wolfgarten, and J. Pollman, J. Phys. C **19**, L141 (1986).

[14] H. J. McSkimin and P. Andreatch, Jr., J. Appl. Phys. **35**, 2161 (1964).

[15] Y. A. Burenkov, S. P. Nikanorov, and A. V. Stepanov, Fiz. Tverd. Tela (Leningrad) **12**, 2428 (1970) [Sov. Phys. Solid State **12**, 1940 (1971)].

[16] L. Kleinman, Phys. Rev. **128**, 2614 (1962).

[17] O. H. Nielsen and R. M. Martin, Phys. Rev. B **32**, 3792 (1985).

[18] C. G. Van de Walle and R. M. Martin, Phys. Rev. B **34**, 5621 (1986).

[19] J. Sánchez-Dehesa, C. Tejeder, and J. A. Vergés, Phys. Rev. B **26**, 5960 (1982).

[20] C. J. Bradley and A. P. Cracknell, *The Mathematical Theory of Symmetry in Solids,* 1st ed. (Clarendon, Oxford, 1972).

[21] W. Harrison, *Electronic Structure and the Properties of Solids* (Freeman, San Francisco, 1980).

[22] S. Y. Ren, J. D. Dow, and D. J. Wolford, Phys. Rev. B **25**, 7661 (1982).

[23] C. Priester, G. Allan, and M. Lannoo, Phys. Rev. B **37**, 8519 (1988).

[24] W. Paul, J. Phys. Chem. Solids **8**, 196 (1959).

[25] I. Balslev, Phys. Rev. **143**, 636 (1966).

[26] J. C. Hensel and G. Feher, Phys. Rev. **129**, 1041 (1963).

[27] L. D. Laude, F. H. Pollak, and M. Cardona, Phys. Rev. B **3**, 2623 (1971).

[28] J. C. Hensel and K. Suzuki, Phys. Rev. B **9**, 4219 (1974).

[29] See, for example, M. Tinkham, *Group Theory and Quantum Mechanics* (McGraw-Hill, New York, 1964).

[30] J. S. Lomont, *Applications for Finite Groups* (Academic, New York, 1959).

[31] *International Tables for Crystallography,* edited by Theo Hahn, Space Group Symmetry Volume A (Reidel, Holland, 1983).

[32] L. P. Bouckaert, R. Smoluchowski, and E. Wigner, Phys. Rev. **50**, 58 (1936).

[33] C. Herring, J. Franklin Inst. **233**, 525 (1942).

[34] G. F. Koster, Solid State Phys. **5**, 173 (1957).

[35] J. Zak, J. Math. Phys. **1**, 165 (1960).

[36] S. C. Miller and W. F. Love, *Tables of Irreducible Representations of Space Groups and Co-representations of Magnetic Space Groups,* 1st ed. (Pruett, Boulder, CO, 1967).

[37] H. A. Kramers, Physica **2**, 483 (1935).

[38] E. P. Wigner, *Group Theory and Its Applications to the Quantum Mechanics of Atomic Spectra* (Academic, New York, 1959).

[39] Q. M. Ma and K. L. Wang, Appl. Phys. Lett. **58**, 1184 (1991).

[40] D. K. Wilson and G. Feher, Phys. Rev. **124**, 1068 (1961).

[41] J. C. Hensel, H. Hasegawa, and M. Nakayama, Phys. Rev. **138**, A225 (1965).

[42] F. Bassani and G. P. Parravicini, *Electronic States and Optical Transitions in Solids,* 1st ed. (Pergamon, Oxford, 1975).